

## Original Article

# Delivery of acetylthevetin B, an antitumor cardiac glycoside, using polymeric micelles for enhanced therapeutic efficacy against lung cancer cells

Jing-jing ZHU<sup>1,2</sup>, Xin-xin ZHANG<sup>2,\*</sup>, Yun-qiu MIAO<sup>2</sup>, Shu-fang HE<sup>2</sup>, Dan-mei TIAN<sup>1</sup>, Xin-sheng YAO<sup>1</sup>, Jin-shan TANG<sup>1,3,\*</sup>, Yong GAN<sup>2,\*</sup>

<sup>1</sup>Institute of Traditional Chinese Medicine and Natural Products, College of Pharmacy, Ji-nan University, Guangzhou 510632, China;

<sup>2</sup>Shanghai Institute of Materia Medica, Chinese Academy of Sciences, Shanghai 201203, China; <sup>3</sup>State Key Laboratory of Drug Research, Shanghai Institute of Materia Medica, Chinese Academy of Sciences, Shanghai 201203, China

### Abstract

Acetylthevetin B (ATB), a cardiac glycoside from the seed of *Thevetia peruviana* (Pers) K Schum (yellow oleander), exhibits not only antitumor activity but also potential cardiac toxicity. In the present study, we attempted to enhance its antitumor action and decrease its adverse effects via chitosan-Pluronic P123 (CP) micelle encapsulation. Two ATB-loaded CP micelles (ATB-CP1, ATB-CP2) were prepared using an emulsion/solvent evaporation technique. They were spherical in shape with a particle size of 40–50 nm, showed a neutral zeta potential, and had acceptable encapsulation efficiency (>90%). Compared to the free ATB (IC<sub>50</sub>=2.94 μmol/L), ATB-loaded CP micelles exerted much stronger cytotoxicity against human lung cancer A549 cells with lower IC<sub>50</sub> values (0.76 and 1.44 μmol/L for ATB-CP1 and ATB-CP2, respectively). After administration of a single dose in mice, the accumulation of ATB-loaded CP1 micelles in the tumor and lungs, respectively, was 15.31-fold and 9.49-fold as high as that of free ATB. A549 xenograft tumor mice treated with ATB-loaded CP1 micelles for 21 d showed the smallest tumor volume (one-fourth of that in the control group) and the highest inhibition rate (85.6%) among all the treatment groups. After 21-d treatment, no significant pathological changes were observed in hearts and other main tissues. In summary, ATB may serve as a promising antitumor chemotherapeutic agent for lung cancer, and its antitumor efficacy was significantly improved by CP micelles, with lower adverse effects.

**Keywords:** cardiac glycoside; acetylthevetin B; antitumor; lung cancer; polymeric micelle; drug delivery; A549 xenograft tumor model

Acta Pharmacologica Sinica (2017) 38: 290–300; doi: 10.1038/aps.2016.113; published online Dec 5 2016

### Introduction

Cardiac glycosides (CGs) are a class of natural products with a steroid-like structure containing an unsaturated lactone ring and a sugar chain, and they are considered amphiphilic molecules<sup>[1]</sup>. CGs are traditionally used in cardiology for the treatment of cardiac congestion and some types of cardiac arrhythmias<sup>[2]</sup>. Recent *in vitro* and *ex vivo* experiments have revealed that several CGs can induce potent and selective anticancer effects at standard therapeutic doses<sup>[3]</sup>. Therefore, CGs may be utilized as anticancer agents. However, many CGs that show strong antitumor activity *in vitro* have not

passed Phase I clinical trials, primarily because the CGs show a lack of tumor selectivity and severe adverse effects, particularly cardiotoxicity<sup>[4,5]</sup>. Therefore, the exploration of effective delivery systems is necessary to enhance the antitumor efficacy and decrease the adverse effects of CGs.

Nanotechnology-based drug delivery systems have received increasing attention because of their ability to load therapeutics and deliver drugs to the site of action, thereby improving the pharmacokinetics of the loaded drugs and reducing off-target toxicity. Among these systems, amphiphilic block co-polymers that spontaneously form self-assembled micellar structures have shown favorable biocompatibility and solubilization effects for amphiphilic drug molecules, including CGs<sup>[6]</sup>. In addition, unlike small molecules, which diffuse in and out of the interstitial space of tumors, nanocarriers (between 10 and 100 nm) have long circulatory properties that enable polymeric micelles to accumulate in tumor tissue via a passive

\*To whom correspondence should be addressed.

E-mail xinxinzhang@simm.ac.cn (Xin-xin ZHANG);

gztangjinshan@126.com (Jin-shan TANG);

simm2122@vip.sina.com (Yong GAN)

Received 2016-07-24 Accepted 2016-10-13

targeting phenomenon, commonly referred to as an enhanced permeability and retention (EPR) effect<sup>[7, 8]</sup>. Inspired by the superiority of nanosized micelles, we intended to deliver CGs to tumor cells using polymeric micelles, which may enhance antitumor efficacy and decrease the cardiotoxicity associated with these drugs.

In a previous study, we observed that acetylthevetin B (ATB), a CG isolated from the seeds of *Thevetia peruviana* (Pers) K Schum (yellow oleander), showed strong cytotoxicity toward three cancer cell lines (human lung cancer cells P15, human gastric cancer cells MGC-803, and human pancreatic cancer cells SW1990) but not toward the normal hepatocyte LO2 cell line<sup>[9]</sup>. To increase targeting potential toward lung cancer and decrease cardiac toxicity, we attempted to establish a nanotechnology-based drug delivery model for ATB. Previous studies have reported the wide exploitation of certain polymeric materials in lung-targeting delivery systems<sup>[7, 10-22]</sup>. Chitosan reportedly exhibits exceptional adhesion ability with lung cancer cells through H-bonding interaction and biotic stickiness<sup>[23-26]</sup>. In addition, Pluronic copolymers, which have a hydrophilic and flexible nature similar to PEG<sup>[27-29]</sup>, are often used to prevent the adsorption of plasma protein, resulting in increased accumulation at the tumor site<sup>[30-34]</sup>. Thus, we sought to exploit and combine the biotic stickiness of chitosan and the enhanced accumulation effect of PEGylation to generate polymer micelles to promote the affinity and cellular uptake of ATB toward lung tumor cells. The cellular uptake, inhibitory effects on A549, *in vitro* cytotoxicity, A549 targeting potential, and *in vivo* antitumor activity of ATB-loaded CP micelles were evaluated.

## Materials and methods

### Materials

Acetylthevetin B (ATB) was obtained from the seeds of *Thevetia peruviana* (Pers) K Schum (yellow oleander)<sup>[9]</sup>, with a purity >98% according to the HPLC analysis (Figure S1-S5).

Pluronic® P123 (PEO<sub>20</sub>-PPO<sub>70</sub>-PEO<sub>20</sub>, MW 5800 Da, PEO 30 wt%) was obtained from Sigma Aldrich (St Louis, MO, USA). Chitosan (CS, MW 10 kDa, deacetylation degree: >90%) was obtained from the Zhejiang Golden Shell Pharmaceutical Co, Ltd (Yuhuan, China). *N,N'*-Disuccinimidyl carbonate (DSC), 4-dimethylaminopyridine (DMAP), coumarin-6, acetonitrile, diethyl ether, isopropanol, and ethanol were obtained from the Sinopharm Chemical Reagent Co, Ltd (Shanghai, China). Hoechst 33342, 3-(4,5-dimethylthiazol-2-yl)-2,5-diphenyltetrazolium bromide (MTT), the cell cycle and apoptosis analysis kit were purchased from the Beyotime Institute of Biotechnology (Shanghai, China). Dulbecco's modified Eagle's medium (DMEM), fetal bovine serum (FBS), penicillin/streptomycin, and 1×trypsin EDTA solution (0.25%, trypsin with 0.53 mmol/L EDTA) were purchased from Life Technologies Co (Grand Island, NY, USA). Alexa Fluor® 555 conjugate WGA and 1,1'-dioctadecyl-3,3',3'-tetramethylindotricarbocyanine iodide (DIR) were obtained from Invitrogen (Carlsbad, CA, USA). The water used for all experiments and analyses was

deionized and filtered using a 0.22-μm pore size polycarbonate syringe filter (Millipore, Billerica, MA). All chemicals were of reagent grade and used without further purification or modification.

### Preparation of ATB-based formulations

ATB-based micelles were prepared using the following procedure. Briefly, 9 μmol of CS, 3 μmol of P123 and 15 mg of ATB were dissolved in 15 mL of ethanol, followed by desiccation and subsequent rehydration at a concentration of 1 mg/mL ATB-CP1 in 15 mL of phosphate-buffered saline (PBS) (pH 7.4). The mixture was homogenized using a high-pressure homogenizer (Nanodebee, South Easton, MA, USA) for three cycles under 600 psi. For ATB-CP2 micelles, 3 μmol of CS and 9 μmol of P123 were used, and all other materials and procedures were the same as described for the preparation of ATB-CP1 micelles.

### Characterization

The particle size distribution and zeta potential of micelles were determined using a Zetasizer Nano ZS analyzer (Malvern, Worcestershire, UK). The micelles were evaluated for shape using transmission electron microscopy (TEM) (Tecnai G2 Spirit Twin, FEI, USA).

The entrapment efficiency (EE, %) was determined using an ultrafiltration-centrifugation technique<sup>[35]</sup>. The recovery of this method was validated. The ATB loaded micelles (500 μL) were placed into filter units (10000 MW, Millipore, Massachusetts, USA) and centrifuged at 3000 r/min for 30 min. Free ATB not incorporated into micelles was separated in the ultrafiltrate. The content of free or total ATB in the micelles was determined using HPLC. Subsequently, the EE% was calculated according to the following Eq:

$$EE\% = \frac{W_T - W_F}{W_T} \times 100\%$$

where  $W_T$  is the weight of total drug in the micelles and  $W_F$  is the weight of free drug in the ultrafiltrate after centrifugation.

The *in vitro* release behavior of ATB from micelles was measured using a dialysis method<sup>[36]</sup>. One milliliter of ATB solution, ATB-CP1, and ATB-CP2 were placed separately into a dialysis tube with a molecular weight cut off of 8000-14000 (Sinopharm Chemical Reagent, Shanghai, China) and dialyzed in 20 mL of PBS (pH 7.4, 37°C). At various times (1, 2, 4, 8, 12, and 24 h), all buffers were replaced with an equal volume of fresh PBS, and the concentration of ATB in the dialysis buffer was analyzed using HPLC.

### Cell line and cell culture

The human lung carcinoma cell line A549 was obtained from the Shanghai Institutes for Biological Sciences. The cells were cultured in DMEM medium with 10% FBS and 0.01% penicillin-streptomycin. The cells were maintained at 37°C in a humidified atmosphere (air supplemented with 5% CO<sub>2</sub>) and passaged using 0.25% trypsin at a subcultivation ratio of 1:3.

### Cellular uptake of ATB-based formulations

To determine the cellular uptake of the micelles, ATB-CP1 and ATB-CP2 micelles were labeled with coumarin-6. First, 0.75 mg of coumarin-6 and CP polymer were dissolved in ethanol, dried to a thin film and subjected to the same procedure as described above (section 2.2, preparation of ATB-based formulations).

For confocal analysis, A549 cells were seeded onto 10 mm<sup>2</sup> glass coverslips in 24-well plates at a density of approximately 1×10<sup>5</sup> cells per well and subsequently incubated for 24 h to enable attachment. The cells were initially incubated with Hoechst 33242 at 37°C to visualize the nuclei. After 30 min of incubation with coumarin-6-labeled CP1 and CP2 micelles, the medium was removed, and the cells were washed three times with PBS. The cells were subsequently incubated with Alexa Fluor<sup>®</sup> 555 conjugate WGA to visualize the membrane. The intracellular distribution of CP micelles was observed using a FluoView FV1000 Confocal Microscope (Olympus, Tokyo, Japan).

The cellular uptake of CP1 and CP2 micelles was measured by flow cytometry (FCM). A549 cells were seeded onto 24-well plate and cultured until a confluent monolayer formed. After removing the culture medium, the cells were incubated with coumarin-6-labeled CP1 and CP2 micelles for 30 min at 37°C. The cells were subsequently washed three times with PBS (pH 7.4), trypsinized, and centrifuged at 2000×g. The harvested cells were re-suspended and analyzed using FACScan flow cytometry (BD, Franklin Lakes, NJ, USA).

### Cytotoxicity assay *in vitro*

To measure the cytotoxicity of ATB solutions and ATB-CP1 and ATB-CP2 micelles, an MTT cell viability assay was performed<sup>[36]</sup>. A549 cells were plated onto 96-well plates at a density of 1×10<sup>4</sup> cells per well and incubated for 24 h to enable attachment. Subsequently, the growth medium was removed, and free ATB, ATB-CP1, and ATB-CP2 micelles at various ATB concentrations of 1, 3, 5, 10, and 20 µg/mL were added. The MTT assay was performed after incubating cells for 24 and 48 h at 37°C.

### Cell cycle analysis

Cell cycle distribution was analyzed through flow cytometry. A549 cells were seeded onto 12-well plates at 1×10<sup>6</sup> cells per well and further incubated for 12 h. A549 cells were treated with free ATB, ATB-CP1, and ATB-CP2 micelles at an ATB concentration of 10 µg/mL for 12 h. The cells were trypsinized, washed three times with PBS, and subsequently fixed in 70% ethanol for at least 1 h at -20°C. The fixed cells were washed with PBS and re-suspended in 0.5 mL propidium iodide (PI) staining solution (69 mmol/L PI, 38 mmol/L sodium citrate and 0.7 mg/mL RNase A, pH 7.4) for 30 min at 37°C in the dark. The stained cells were processed through flow cytometry.

### Animals

Male BALB/c *nu/nu* nude mice (4–6 weeks old, 20±2 g) were

obtained from the Animal Facility of the Shanghai Institute of Materia Medica (Shanghai, China) and housed in a 12-h/12-h light-dark cycle at a room temperature of 23±2°C with a relative humidity of 55%±15%. Food and water were provided *ad libitum* throughout the acclimatization and experimental periods. The animal experiments were reviewed and approved through the Institutional Animal Care and Use Committee (IACUC) of the Shanghai Institute of Materia Medica, Chinese Academy of Sciences, Shanghai, China.

### Examination of biodistribution through *in vivo* imaging

A549 cells (5×10<sup>6</sup> cells) were subcutaneously (sc) implanted into the fourth mammary fat pads of 4–6 weeks old male BALB/c *nu/nu* nude mice to establish xenograft tumors. Two weeks after tumor implantation, the mice were randomized into three treatment groups of free ATB, ATB-CP1, and ATB-CP2 micelles (3 mice per group).

The biodistribution of free ATB, ATB-CP1, and ATB-CP2 micelles was analyzed using a non-invasive *in vivo* optical imaging technique<sup>[37]</sup>. The mice were treated with NIR fluorescent-labeled ATB and micelles. DIR, a recently introduced carbocyanine lipophilic NIR fluorescent membrane dye, was used to label the free ATB and micelles<sup>[38]</sup>. DIR-labeled ATB solution was prepared by dissolving 0.25 mg of DIR and 12.5 mg of ATB in 2.5 mL of ethanol, followed by dilution at a concentration of 5 mg/mL ATB in 50 mL of saline. DIR-labeled micelles were prepared by dissolving DIR, ATB and polymers in ethanol, followed by drying to a thin film, according to the procedure described above (section 2.2, preparation of ATB-based formulations). The final concentration of DIR was 100 µg/mL in each formulation.

Free DIR, DIR-ATB, and DIR-labeled micelles (DIR-ATB-CP1 and DIR-ATB-CP2) were administered through intravenous (iv) injection by tail (10 µg DIR of each mouse). At 15 min and 6 h post injection, the biodistributions of DIR-labeled formulations in live (15 min and 6 h post injection) and euthanized animals (6 h post injection) were investigated using the IVIS<sup>®</sup> Spectrum System (Caliper Cor, Waltham, Massachusetts, USA). The excitation and emission wavelengths were 745 and 800 nm, respectively.

The results were analyzed using Living Image<sup>®</sup> Software Version 4.3.1 (Caliper Corp, Waltham, Massachusetts, USA). All experiments were repeated in three different animals, and representative pictures are shown<sup>[19]</sup>.

### *In vivo* antitumor activity and cytotoxicity in an A549 xenograft model

A549 cells (5×10<sup>6</sup> cells) were implanted (sc) into the fourth mammary fat pads of 4–6-week-old male BALB/c *nu/nu* nude mice to establish xenograft tumors. Two weeks after tumor implantation, the mice were randomly divided into four groups (6 mice per group; free ATB, ATB-CP1, ATB-CP2 and control) and administered ATB-based formulations for 3 weeks. The drug-treated groups received 1.5 mg/kg of ATB through iv injection via the tail vein every 3 d. The control mice received the same volume of physiological saline. The

body weights were monitored every 3 d. The tumor-bearing mice were euthanized through CO<sub>2</sub> asphyxiation on d 22, and the livers were excised. The tumors were detached and weighed, and the tumor volume was determined using a slide gauge according to the following formula<sup>[39]</sup>:

$$\text{Volume (mm}^3\text{)} = (\text{length} \times \text{width}^2) / 2$$

Tumor tissues were removed from the euthanized mice and weighed to calculate the tumor inhibition rate:

$$\text{TIR (\%)} = (1 - W_t / W_c) \times 100\%$$

where  $W_t$  and  $W_c$  are the mean tumor weights of the treated groups and the negative control group, respectively. Moreover, the main tissues, including heart, liver, spleen, lung, and kidney, were rinsed with normal saline, fixed in 10% formalin, and subsequently embedded in paraffin blocks for slicing and staining with hematoxylin and eosin (H&E). The sections were observed under a microscope for histopathological evaluation<sup>[40]</sup>.

### Statistical analysis

The data from each treatment and control group are present as the mean ± SD. Statistical analysis was performed using Student's *t*-test and ANOVA.

## Results

### Characterization of ATB-loaded micelles

The ATB concentration in ATB-CP1 and ATB-CP2 micelles was 1 mg/mL. The physicochemical characteristics and entrapment efficiency (EE, %) parameters for ATB-CP1 and ATB-CP2 are summarized in Table 1. The two types of micelles had a mean particle size of approximately 40–50 nm. All formulations exhibited a similar neutral surface charge (~0 mV). ATB was encapsulated into the two different micelles with high EE% of >90%. As presented in Figure 1A, the micelles imaged using TEM had spherical shapes, and the size correlated well with the results of laser diffraction (Table 1).

In the present study, PBS was applied as the release medium. The *in vitro* cumulative release profiles of ATB from different formulations are shown in Figure 1B. The free ATB released from the solution was investigated as a control. The results showed that approximately 100% ATB in the stock solution was released within 4 h, suggesting that ATB could freely diffuse through the dialysis membrane. The 4-h cumulative ATB release from ATB-CP1 was 60.3% ± 0.9%, compared with 50.3% ± 2.5% for ATB-CP2, suggesting the prolonged release of ATB from the micelle preparation.

**Table 1.** Characterization of acetylthevetin B (ATB)-based formulations. Mean ± SD. *n* = 3.

Formulations	Particle size (nm)	Zeta potential (mV)	EE%
ATB-CP1	50.69 ± 3.12	-2.50 ± 1.82	93.8 ± 0.25
ATB-CP2	39.91 ± 5.27	-7.36 ± 3.81	90.1 ± 0.21

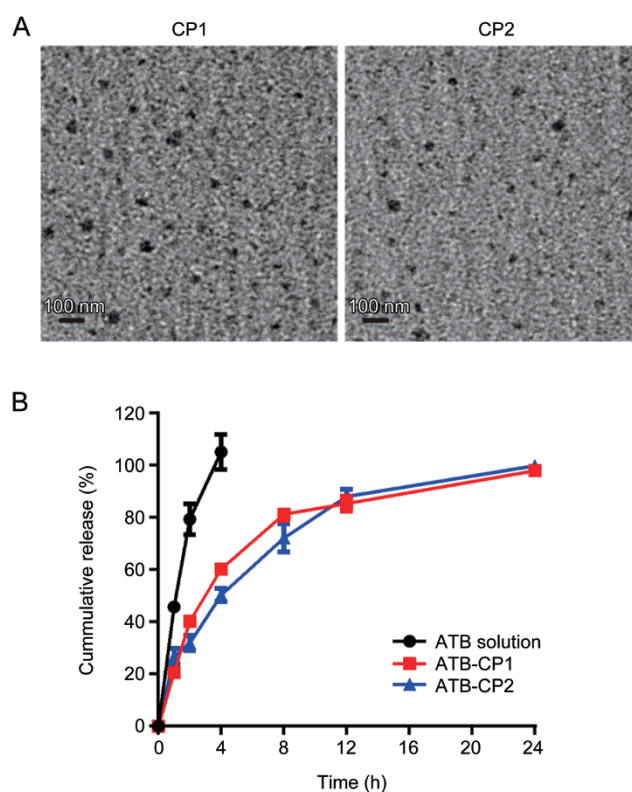


**Figure 1.** (A) Transmission electron microscopy (TEM) images of CP1 and CP2 micelles. (B) Release profile of acetylthevetin B (ATB) from free ATB, ATB-CP1, and ATB-CP2 in phosphate buffer solution (PBS) (pH 7.4) at 37 °C.

### Cellular uptake of micelles

To investigate the cellular uptake of ATB-based formulations, A549 lung tumor cells were incubated with coumarin-6 labeled CP micelles, followed by confocal microscopy and quantitative analysis using flow cytometry. The nuclei were stained with Hoechst. The green fluorescence showed the micelle uptake by the cells, and the membranes were stained with red. As shown in Figure 2, the CP micelles distributed in the cytoplasm after intake by A549 cells. CP1 showed stronger colocalization with the membrane of A549 cells compared to CP2. The CP1 uptake in A549 cells was markedly higher than that of CP2. The mean fluorescent intensity of CP1 micelles in A549 was 2.82 times higher than that of CP2, with a statistical significant difference between CP1 and CP2 (733.33 vs 260.00,  $P < 0.01$ ).

### Enhanced cytotoxicity and apoptosis of A549 cells induced through ATB-based formulations

The above data demonstrates that ATB-CP1 could enhance cellular uptake in A549 cells. As a result, the delivery of ATB with CP1 micelles can markedly increase the concentration of the free drug in A549 cells, thereby increasing drug cytotoxicity. To determine the cytotoxic effects, we incubated free ATB, ATB-CP1, and ATB-CP2 with A549 cells. All ATB formulations showed dose-dependent and time-dependent

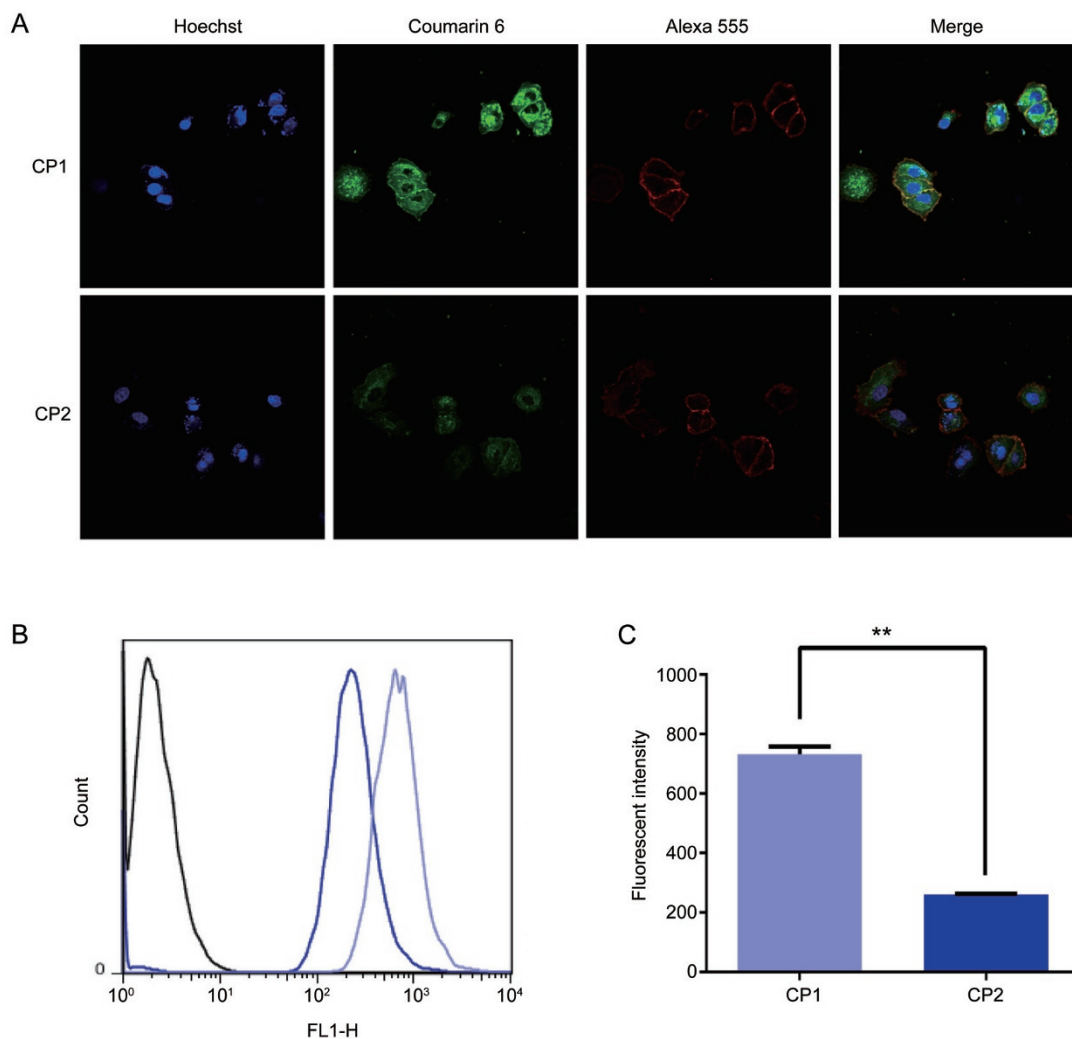


**Figure 2.** (A) Confocal microscopy images of A549 cells after 30 min incubation with coumarin-6 labeled CP1 and CP2 micelles and the correlation scatter plot of the intensities of coumarin-6 and Alexa Fluor® 555 WGA. (B) The cellular uptake of CP1 micelles are shown in light blue and the cellular uptake of CP2 micelles are shown in dark blue while the black line represents the negative control. (C) Quantitative analysis of cellular uptake by flow cytometry. The error is the standard deviation from the mean.  $n=3$ . \*\* $P<0.01$ .

toxicity (Figure 3A, 3B). In addition, free ATB showed obvious cytotoxicity against A549 cells ( $IC_{50}=2.94 \mu\text{mol/L}$ ) after incubation for 48 h, and ATB-CP1 had significantly increased cytotoxicity ( $IC_{50}=0.76 \mu\text{mol/L}$ ) compared with free ATB and ATB-CP2 ( $IC_{50}=1.44 \mu\text{mol/L}$ ). This finding might result from the enhanced cellular ATB retention.

To evaluate the mechanism of cytotoxic effects, the DNA content of A549 cells (after treatment with various formulations) was examined using FCM to assess cell cycle progression. As shown in Figure 3C, the cell cycle distribution revealed that 50.18% of the control cells were in  $G_0/G_1$  phase, whereas the  $G_0/G_1$  population decreased to 49.68%, 21.46%, and 40.92% for the free ATB solution, ATB-CP1, and ATB-CP2, respectively. Moreover, 32.98% of the control cells were in the S phase, close to the 26.28% of free ATB solution-treated cells, whereas the S population increased to 55.61% and 56.01% for ATB-CP1 and ATB-CP2, respectively.

#### Biodistribution of micelles in mice bearing orthotopic xenograft tumors

DIR integrates with high stability into micelles and remains attached, even when in contact with other membranes. To determine the real-time biodistribution of micelles, free DIR solution, DIR-labeled free ATB (DIR is an amphiphilic material similar to ATB, which micellizes with ATB; its amount in formulation is controlled at far below the amount of ATB to ensure that the distribution of this formulation could reflect the distribution of free ATB), and micelles were intravenously injected into mice bearing A549 orthotopic xenograft tumor; the *in vivo* targeting efficacy of the formulations was observed using non-invasive NIRF imaging in live animals (Figure 4A). The selected ICG filter facilitated the precise detection of the DIR fluorophore, as all autofluorescence signals were effectively blocked (Figure 4A and 4B). After the iv administration of DIR-labeled formulations, a strong NIRF signal from DIR-

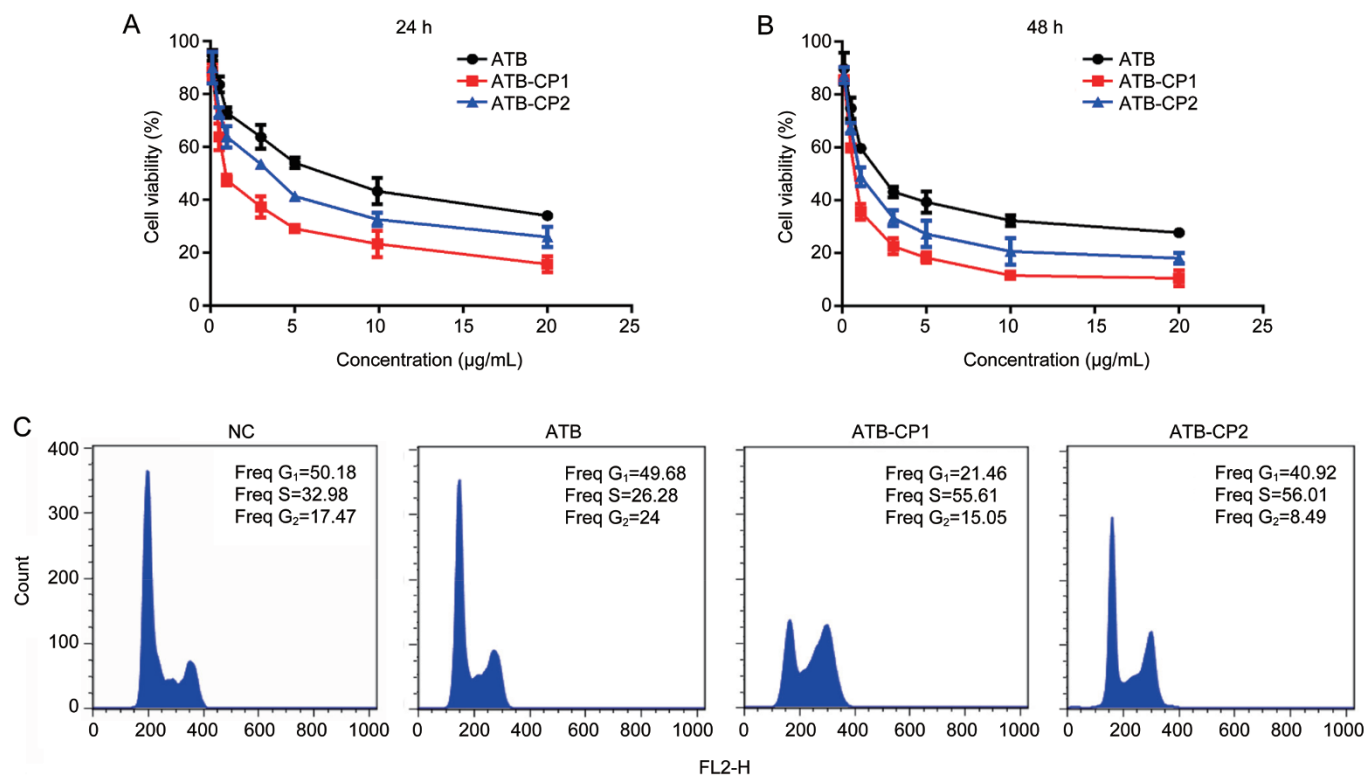


**Figure 3.** *In vitro* cytotoxicity of free acetylthevetin B (ATB), ATB-CP1, and ATB-CP2 against A549 cells. Cell viability of A549 cells after incubating with free ATB, ATB-CP1, and ATB-CP2 at different concentrations for 24 h (A) and 48 h (B). (C) Cell cycle distribution of A549 cells treated with ATB solution, ATB-CP1, and ATB-CP2 at a concentration of 10 µg/mL for 12 h by flow cytometry.

ATB-CP1 and DIR-ATB-CP2 micelles was observed in the tumor (the position of the tumor is shown as a black circle in Figure 4A), whereas fewer signals from the free DIR solution and DIR-labeled free ATB solution could be observed in the orthotopic xenograft tumor. At the 6-h time point, no obvious NIRF signal from the ATB solution was observed in the tumor, whereas DIR-ATB-CP1 and DIR-ATB-CP2 micelles remained accumulated at the tumor site.

For a more accurate measurement, major internal organs (heart, liver, spleen, lung, and kidney) were removed at 6 h post injection and analyzed directly using a fluorescent imager (Figure 4B). The mean fluorescent intensity concentration of DIR-ATB-CP1 micelles ( $14.24 \times 10^9/g$ ) in the A549 solid tumor increased approximately 15.31-fold compared with the free ATB solution ( $0.93 \times 10^9/g$ ) and 2.24-fold compared with DIR-ATB-CP2 micelles ( $6.36 \times 10^9/g$ ). However, the distribution in the lungs requires further attention, as this distribution reflects the organ selectivity of the formulations. DIR-ATB-CP1 micelles ( $30.75 \times 10^9/g$ ) showed a 9.49-fold increase in fluorescent intensity compared to the free ATB solution ( $3.24 \times 10^9/g$ ) in the lungs. The fluorescent intensity of DIR-ATB-CP1 micelles in the lungs was 2.21-fold higher than that of DIR-ATB-CP2 micelles. Importantly, the distribution of DIR-ATB-CP1 micelles in the heart ( $1.32 \times 10^9/g$ ) was significantly less than that of free ATB ( $4.39 \times 10^9/g$ , 3.33-fold) and DIR-ATB-CP2 micelles ( $2.48 \times 10^9/g$ , 1.88-fold) ( $P < 0.01$ ).

#### Antitumor efficacy and toxicity of ATB-based formulations

The antitumor activity of free ATB, ATB-CP1, and ATB-CP2 was validated using the A549 xenograft tumor model in BALB/c nude mice. As shown in Figure 5A, the tumor volume of the control group exhibited linear growth in the later period indicating a high degree of malignancy. Compared with the control, tumor growth was inhibited in all the groups treated with ATB formulations. ATB-CP1 demonstrated the highest inhibitory effect on tumor growth compared to control, and the tumor volume significantly decreased from ( $436.48 \pm 34.93$ ) mm<sup>3</sup> to ( $106.5 \pm 9.79$ ) mm<sup>3</sup> (4.10-fold decrease compared to the control group). In addition, ATB-CP1 also showed the lowest tumor volume compared with free ATB solution and ATB-CP2 micelles. The pictures of the tumors from each group are shown in Figure 5D, and the tumor volume of the ATB-CP1 group was the smallest among the treatment groups. In addition, the tumor weight at the end of the experiment showed the same trend. The inhibition rates for free ATB solution, ATB-CP1, and ATB-CP2 were 43.8%, 85.6%, and 59.7%, respectively, compared to the control group. The ATB-CP1 group showed the lowest tumor weight and the highest inhibition rate among all treatment groups (Figure 5C).

At the end of the experiment, the tumors were removed and sectioned for pathological analysis. Histological examination of the tumor tissues from each group further confirmed the

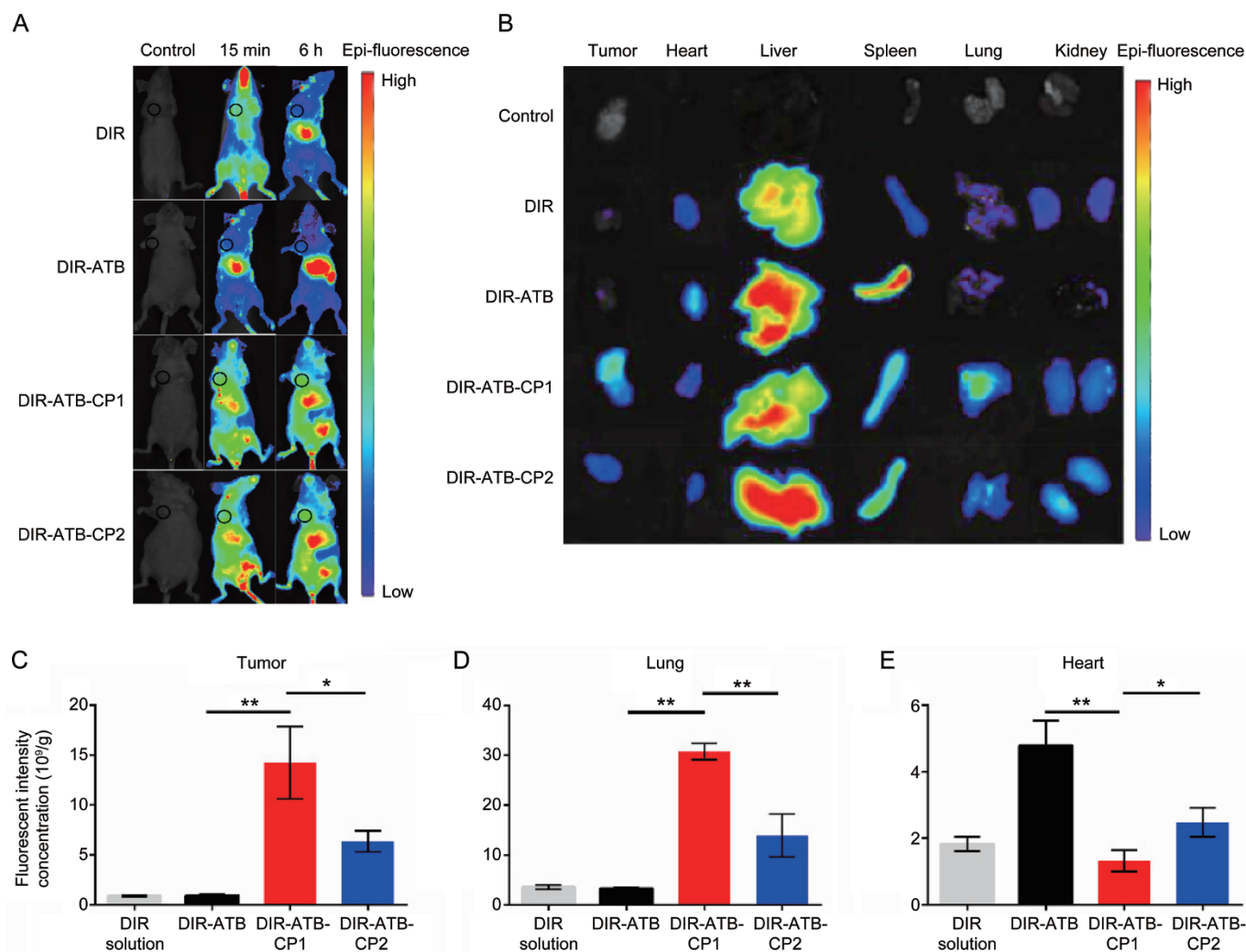


**Figure 4.** Biodistribution of 1,1'-dioctadecyl-3,3,3',3'-tetramethylindotricarbocyanine iodide (DIR)-labeled formulations after intravenous (iv) injection in mice. (A) Real-time *in vivo* fluorescence images of mice after iv injection of free DIR, DIR labeled acetylthevetin B (ATB) solution (DIR-ATB), DIR-labeled CP1 (DIR-ATB-CP1), and DIR-labeled CP2 (DIR-ATB-CP2) ( $\lambda_{ex}=745$  nm;  $\lambda_{em}=800$  nm). (B) Fluorescence images of organs excised at 6 h post injection. Biodistribution of DIR-labeled formulations in tumor (C), lung (D), and heart (E) excised from mice at 6 h post injection. The error is the standard deviation from the mean.  $n=3$ . \* $P<0.05$ , \*\* $P<0.01$ .

successful destruction of tumor cells by ATB-CP1. As shown in Figure 5E, the tumor tissue treated with normal saline revealed malignancy. The nuclei of the cancer cells were large and oval-shaped, with increased chromatin and visible binucleolates. In contrast, tumor sections treated with ATB-CP1 clearly showed severe apoptosis across a large tumor area. In

mice injected with ATB-CP2, tumor apoptosis was somewhat increased beyond that in ATB-treated mice, but this effect was not as significant as observed in mice treated with ATB-CP1. These findings suggested that ATB-CP1 exhibited the greatest therapeutic efficacy among all treatment groups.

After 21 d of treatment, the survival rates of each group were 100%. The body weight of mice is shown in Figure 6B, and no significant body weight loss was observed in mice injected with free ATB, ATB-CP1, and ATB-CP2 during the treatment. Based on the results of the QPatch™ assay of ATB toward the potassium channel, the cardiotoxicity of ATB was far less than that of cisapride (a positive control). However, the toxicity of ATB toward CHO-hERG cells indicated that this compound might cause weak cardiotoxicity because the inhibition rate of the ATB group was higher than that of digoxin (Table S1, S2). Histopathological evaluation was required to

**Table 2.** IC<sub>50</sub> value of free acetylthevetin B (ATB), ATB-CP1, and ATB-CP2 against A549 cells.  $n=3$ . Mean±SD.

Formulations	24 h (μmol/L)	48 h (μmol/L)
ATB	7.22±0.29	2.94±0.17
ATB-CP1	1.40±0.09	0.76±0.10
ATB-CP2	3.40±0.12	1.44±0.21

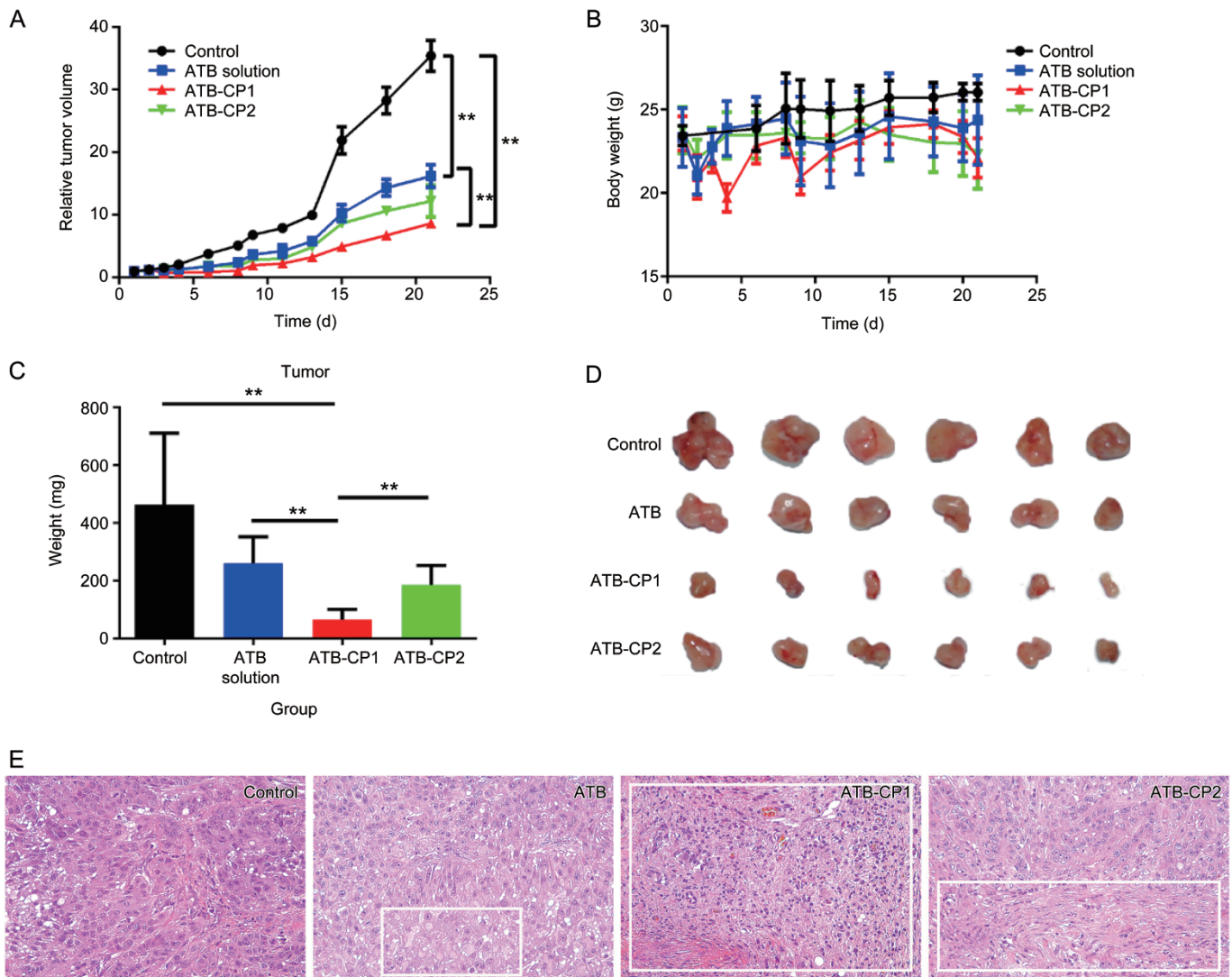


**Figure 5.** Effect of intravenous (iv) injection of acetylthevetin B (ATB)-based formulations on tumor growth in BALB/c nude mice with A549 drug resistant xenograft tumors. (A) The average values of the relative tumor volume  $V/V_0$ . Each data point represents the mean $\pm$ SD of 6 different mice.  $^{**}P<0.01$ , significantly different from the ATB or control injection group. (B) Body weights of the mice over the experimental period.  $n=6$ . (C) Tumor weight after 21 d of treatment with the ATB solution, ATB-CP1, or ATB-CP2.  $n=6$ .  $^{**}P<0.01$ . (D) Tumor pictures of the mice treated with free ATB, ATB-CP1, and ATB-CP2. (E) Hematoxylin and eosin (H&E) stained tumor slices from mice on d 22 after treatments with saline, free ATB, ATB-CP1, and ATB-CP2. Images were obtained under Leica DMRE light microscopy using a 400 $\times$  objective.

confirm the toxicity of ATB on rat hearts and other tissues. Representative pathological images of the hearts and other tissues are presented in Figure 6 and Figure S6–S9. Notably, after treatment for 21 d, no significant pathological changes were observed in the hearts and other main tissues in all treatment groups. These results suggest that all ATB-based formulations have relatively weak toxic effects on the heart and other main tissues.

## Discussion

ATB is a typical CG containing a hydrophobic steroidal aglycone and hydrophilic glycosyl functionality, which confers its amphiphilic nature<sup>[3, 41, 42]</sup>. For the driving force of micellization, Pluronic copolymers consist of hydrophilic poly(ethylene

oxide) (PEO) and hydrophobic poly(propylene oxide) (PPO) tri-block structures; thus, the driving force is the hydrophobic interaction between PPO blocks<sup>[28]</sup>. The particle sizes were correlated well with Pluronic-type micelles, whose average hydrodynamic diameter ranged from 20 to 80 nm<sup>[43]</sup>. For the *in vitro* cumulative release profiles of the ATB formulations, the steric protection effect of the PEO-PPO-PEO chain on the surface of micelles minimizes premature drug leakage, enabling the accumulation of drug molecules at the targeted site<sup>[44]</sup>.

In the cellular uptake study, the results indicated that the transportation of ATB across the A549 cell membrane can be markedly improved by CP1 micelles, and higher cellular accumulation of the drug will be reached. The cytotoxic studies suggested that all ATB formulations induced the arrest of

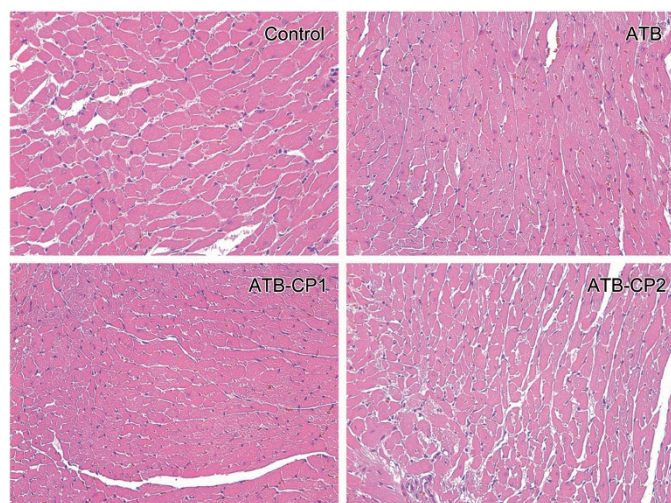


**Figure 6.** Hematoxylin and eosin (H&E) stained heart slices from mice on d 22 after treatments with saline, free ATB, ATB-CP1, and ATB-CP2. Images were obtained under Leica DMRE light microscopy using a 400× objective.

cell growth at different levels, indicating that ATB has anti-tumor activity, with ATB-CP1 exhibiting superior efficacious S-phase arrest and a significant reduction in the  $G_0/G_1$  phase. These findings demonstrated that CP1 micelles significantly improved the membrane transportation ability of ATB. Thus, the enhanced accumulation of cellular ATB played a pivotal role in enhancing cell cycle arrest, which is consistent with the *in vitro* cytotoxicity results.

Furthermore, we used an A549 xenograft tumor model in BALB/c nude mice to study the antitumor activity of ATB *in vivo*. The biodistribution study suggested that the distribution of ATB could be changed by CP1 micelles, and its distribution in solid tumors and the lungs could be largely improved through CP1. In addition, the decreased amount of CP1 in the heart indicated that the cardiac toxicity of ATB might be decreased to some extent. The prolonged tumor inhibition effect of ATB and its formulations was evaluated, and the results indicated that ATB-CP1 exhibited the strongest antitumor activity toward A549 solid tumors. The cellular uptake and distribution of ATB in tumor and lung tissues were enhanced by the affinity toward A549 cells and the EPR effect<sup>[7, 8]</sup> of micelles. The CP1 package also decreased the distribution of ATB in the heart, liver and spleen. Thus, the *in vivo* antitumor efficacy of ATB was markedly enhanced without significant toxicity in normal tissues. Previous studies have reported that the affinity of nanocarriers for cells or organs may attribute to their interaction with cell membranes<sup>[30–34]</sup>. Moreover, this effect is conducive for ATB to play a strong tumor curative effect in lung cancer.

The CP1 micelle, reflecting its strong affinity toward the A549 cell membrane, increased the intracellular ATB concentration to levels exceeding that of free ATB or the drug being delivered by the CP2 micelle. Moreover, ATB and its formulation ATB-CP1 were preliminarily confirmed to induce no

significant damage to main organ tissues after 21 d of treatment. Studies on the long-term effects of ATB toward normal organs are still required. From a clinical viewpoint, ATB-CP1 exhibited high antitumor efficacy and low cytotoxicity *in vivo* and may serve as an antitumor formulation for the treatment of lung cancer.

In summary, we have successfully prepared CG formulations for the treatment of lung cancer. ATB was successfully loaded in a biofunctionalized polymeric micelle, and its anti-tumor activity and cytotoxicity were evaluated *in vitro* and *in vivo*. The ability of ATB to transport across the A549 cell membrane was improved by the CP1 micelle, leading to the increased cellular accumulation of the drug. In A549 cells, the antitumor efficacy of ATB was enhanced by the formulation. In A549 cell tumor-bearing mice, the results of the biodistribution study showed that the CP1 micelle could enhance the retention time and concentration of ATB in tumor tissue, and reduce its distribution in the heart. In the *in vivo* study, ATB-CP1, benefiting from the strong affinity of CP1 towards tumor cells, showed markedly improved therapeutic effects and no apparent side effects. Based on these findings, we anticipate the contribution of the CP1 micelle to the development of CGs in clinical applications. However, the total synthesis and specific anti-tumor mechanism of ATB should be further studied for the future application of this compound.

### Acknowledgements

Financial support was obtained from the National Natural Science Foundation of China (No 81571796, 81673320), the Youth Innovation Promotion Association (No 2015229), the SA-SIBS Scholarship Program, and the State Key Laboratory of Drug Research (No SIMM1403KF-15 and SIMM1601KF-09). The authors would like to thank Dr Zhuang WEI for generously providing lung carcinoma A549 cells.

### Author contribution

Jing-jing ZHU performed most of the experiments and drafted the manuscript. Xin-xin ZHANG modified the technical aspects of the manuscript. Yun-qiu MIAO assisted in the cell culture experiments. Shu-fang HE assisted in the analysis of the cell culture results. Dan-mei TIAN and Xin-sheng YAO assisted in the extraction, isolation and characterization of ATB. Xin-xin ZHANG, Jin-shan TANG, and Yong GAN designed and directed the study and participated in the overall editing and approval of the paper. All authors reviewed the manuscript.

### Supplementary information

The chemical structure of ATB, HRESIMS,  $^1\text{H}$  and  $^{13}\text{C}$  NMR spectra, signal assignment of ATB, and other information are provided in the supporting information at the website of Acta Pharmacologica Sinica.

### References

- 1 Prassas I, Diamandis EP. Novel therapeutic applications of cardiac glycosides. *Nat Rev Drug Discov* 2008; 7: 926–35.

- 2 Newman RA, Yang PY, Pawlus AD, Block KI. Cardiac glycosides as novel cancer therapeutic agents. *Mol Interv* 2008; 8: 36–49.
- 3 Haux J. Digitoxin is a potential anticancer agent for several types of cancer. *Med Hypotheses* 1999; 53: 543–8.
- 4 Zhang HY, Xu WQ, Wang YW, Omari-Siaw E, Wang Y, Zheng YY, et al. Tumor targeted delivery of octreotide-periplogenin conjugate: synthesis, *in vitro* and *in vivo* evaluation. *Int J Pharm* 2016; 502: 98–106.
- 5 Tian X, Yin H, Zhang S, Luo Y, Xu K, Ma P, et al. Bufalin loaded biotinylated chitosan nanoparticles: an efficient drug delivery system for targeted chemotherapy against breast carcinoma. *Eur J Pharm Biopharm* 2014; 87: 445–53.
- 6 Biswas S, Kumari P, Lakhani PM, Ghosh B. Recent advances in polymeric micelles for anti-cancer drug delivery. *Eur J Pharm Sci* 2016; 83: 184–202.
- 7 Wang X, Yang C, Zhang Y, Zhen X, Wu W, Jiang X. Delivery of platinum (IV) drug to subcutaneous tumor and lung metastasis using bradykinin-potentiating peptide-decorated chitosan nanoparticles. *Biomaterials* 2014; 35: 6439–53.
- 8 Liu J, Jiang ZZ, Zhang SM, Saltzman WM. Poly(omega-pentadecalactone-co-butylene-co-succinate) nanoparticles as biodegradable carriers for camptothecin delivery. *Biomaterials* 2009; 30: 5707–19.
- 9 Tian DM, Cheng HY, Jiang MM, Shen WZ, Tang JS, Yao XS. Cardiac glycosides from the seeds of *Thevetia peruviana*. *J Nat Prod* 2016; 79: 38–50.
- 10 Sadhukha T, O'Brien TD, Prabha S. Nano-engineered mesenchymal stem cells as targeted therapeutic carriers. *J Control Release* 2014; 196: 243–51.
- 11 Naguib YW, Rodriguez BL, Li X, Hursting SD, Williams RO 3rd, Cui Z. Solid lipid nanoparticle formulations of docetaxel prepared with high melting point triglycerides: *in vitro* and *in vivo* evaluation. *Mol Pharm* 2014; 11: 1239–49.
- 12 Ganesh S, Iyer AK, Morrissey DV, Amiji MM. Hyaluronic acid based self-assembling nanosystems for CD44 target mediated siRNA delivery to solid tumors. *Biomaterials* 2013; 34: 3489–502.
- 13 Ganesh S, Iyer AK, Gattacceca F, Morrissey DV, Amiji MM. *In vivo* biodistribution of siRNA and cisplatin administered using CD44-targeted hyaluronic acid nanoparticles. *J Control Release* 2013; 172: 699–706.
- 14 Karra N, Nassar T, Ripin AN, Schwob O, Borlak J, Benita S. Antibody conjugated PLGA nanoparticles for targeted delivery of paclitaxel palmitate: efficacy and biofate in a lung cancer mouse model. *Small* 2013; 9: 4221–36.
- 15 Haisung L, Dong Kee Y. A study of Gd loaded silica nanoparticles for both optical and magnetic resonance imaging of cells. *Mater Lett* 2013; 100: 98–101.
- 16 Tobin LA, Xie Y, Tsokos M, Chung SI, Merz AA, Arnold MA, et al. Pegylated siRNA-loaded calcium phosphate nanoparticle-driven amplification of cancer cell internalization *in vivo*. *Biomaterials* 2013; 34: 2980–90.
- 17 Ruiz A, Hernandez Y, Cabal C, Gonzalez E, Veintemillas-Verdaguer S, Martinez E, et al. Biodistribution and pharmacokinetics of uniform magnetite nanoparticles chemically modified with polyethylene glycol. *Nanoscale* 2013; 5: 11400–8.
- 18 Ruiz A, Salas G, Calero M, Hernandez Y, Villanueva A, Herranz F, et al. Short-chain PEG molecules strongly bound to magnetic nanoparticle for MRI long circulating agents. *Acta Biomater* 2013; 9: 6421–30.
- 19 Zhang XX, Guo SY, Fan R, Yu MR, Li FF, Zhu CL, et al. Dual-functional liposome for tumor targeting and overcoming multidrug resistance in hepatocellular carcinoma cells. *Biomaterials* 2012; 33: 7103–14.
- 20 Wei PR, Cheng SH, Liao WN, Kao KC, Weng CF, Lee CH. Synthesis of chitosan-coated near-infrared layered double hydroxide nanoparticles for *in vivo* optical imaging. *J Mater Chem* 2012; 22: 5503–13.
- 21 Esmaeili F, Dinarvand R, Ghahremani MH, Ostad SN, Esmaily H, Atyabi F. Cellular cytotoxicity and *in-vivo* biodistribution of docetaxel poly(lactide-co-glycolide) nanoparticles. *Anti-Cancer Drug* 2010; 21: 43–52.
- 22 Hwang HY, Kim IS, Kwon IC, Kim YH. Tumor targetability and anti-tumor effect of docetaxel-loaded hydrophobically modified glycol chitosan nanoparticles. *J Control Release* 2008; 128: 23–31.
- 23 Ladet S, David L, Domard A. Multi-membrane hydrogels. *Nature* 2008; 452: 76–9.
- 24 Pavinatto FJ, Pavinatto A, Caseli L, dos Santos DS, Nobre TM, Zaniquelli MED, et al. Interaction of chitosan with cell membrane models at the air-water interface. *Biomacromolecules* 2007; 8: 1633–40.
- 25 Khor E, Lim LY. Implantable applications of chitin and chitosan. *Biomaterials* 2003; 24: 2339–49.
- 26 Huang M, Ma Z, Khor E, Lim LY. Uptake of FITC-chitosan nanoparticles by A549 cells. *Pharm Res* 2002; 19: 1488–94.
- 27 Otsuka H, Nagasaki Y, Kataoka K. PEGylated nanoparticles for biological and pharmaceutical applications. *Adv Drug Deliver Rev* 2012; 64: 246–55.
- 28 Kabanov AV, Lemieux P, Vinogradov S, Alakhov V. Pluronic block copolymers: novel functional molecules for gene therapy. *Adv Drug Deliv Rev* 2002; 54: 223–33.
- 29 Barreto JA, O'Malley W, Kubeil M, Graham B, Stephan H, Spiccia L. Nanomaterials: applications in cancer imaging and therapy. *Adv Mater* 2011; 23: H18–40.
- 30 Pelaz B, del Pino P, Maffre P, Hartmann R, Gallego M, Rivera-Fernandez S, et al. Surface functionalization of nanoparticles with polyethylene glycol: effects on protein adsorption and cellular uptake. *ACS Nano* 2015; 9: 6996–7008.
- 31 Dai Q, Walkey C, Chan WCW. Polyethylene glycol backfilling mitigates the negative impact of the protein corona on nanoparticle cell targeting. *Angew Chem Int Edit* 2014; 53: 5093–6.
- 32 Treuel L, Brandholt S, Maffre P, Wiegele S, Shang L, Nienhaus GU. Impact of protein modification on the protein corona on nanoparticles and nanoparticle-cell interactions. *ACS Nano* 2014; 8: 503–13.
- 33 Torrisi V, Graillot A, Vitorazi L, Crouzet Q, Marletta G, Loubat C, et al. Preventing corona effects: multiphosphonic acid poly(ethylene glycol) copolymers for stable stealth iron oxide nanoparticles. *Biomacromolecules* 2014; 15: 3171–9.
- 34 Walkey CD, Olsen JB, Guo H, Emili A, Chan WC. Nanoparticle size and surface chemistry determine serum protein adsorption and macrophage uptake. *J Am Chem Soc* 2012; 134: 2139–47.
- 35 Zhuang CY, Li N, Wang M, Zhang XN, Pan WS, Peng JJ, et al. Preparation and characterization of vinpocetine loaded nanostructured lipid carriers (NLC) for improved oral bioavailability. *Int J Pharm* 2010; 394: 179–85.
- 36 Rudra A, Deepa RM, Ghosh MK, Ghosh S, Mukherjee B. Doxorubicin-loaded phosphatidylethanolamine-conjugated nanoliposomes: *in vitro* characterization and their accumulation in liver, kidneys, and lungs in rats. *Int J Nanomed* 2010; 5: 811–23.
- 37 Morgan NY, English S, Chen W, Chernomordik V, Russo A, Smith PD, et al. Real time *in vivo* non-invasive optical imaging using near-infrared fluorescent quantum dots 1. *Acad Radiol* 2005; 12: 313–23.
- 38 Christian DA, Garbuzenko OB, Minko T, Discher DE. Polymer vesicles with a red cell-like surface charge: microvascular imaging and *in vivo* tracking with near-infrared fluorescence. *Macromol Rapid Comm* 2010; 31: 135–41.
- 39 Michaelis M, Zimmer A, Handjou N, Cinatl J, Cinatl J. Increased

- systemic efficacy of aphidicolin encapsulated in liposomes. *Oncol Rep* 2005; 13: 157–60.
- 40 Lo A, Lin CT, Wu HC. Hepatocellular carcinoma cell-specific peptide ligand for targeted drug delivery. *Mol Cancer Ther* 2008; 7: 579–89.
- 41 McConkey DJ, Lin Y, Nutt LK, Ozel HZ, Newman RA. Cardiac glycosides stimulate  $Ca^{2+}$  increases and apoptosis in androgen-independent, metastatic human prostate adenocarcinoma cells. *Cancer Res* 2000; 60: 3807–12.
- 42 Yeh JY, Huang WJ, Kan SF, Wang PS. Inhibitory effects of digitalis on the proliferation of androgen dependent and independent prostate cancer cells. *J Urol* 2001; 166: 1937–42.
- 43 Nagarajan R. Solubilization of hydrocarbons and resulting aggregate shape transitions in aqueous solutions of Pluronic (R) (PEO-PPO-PEO) block copolymers. *Colloid Surface B* 1999; 16: 55–72.
- 44 Alvarez-Lorenzo C, Sosnik A, Concheiro A. PEO-PPO block copolymers for passive micellar targeting and overcoming multidrug resistance in cancer therapy. *Curr Drug Targets* 2011; 12: 1112–30.